remote sensing

MDPI

Article

Validation of CrIS Radiometric Performance through Its Comparison to ABI

Zhipeng Wang [1], Flavio Iturbide-Sanchez [2,*], Peter Beierle [3], Kun Zhang [4] and Denis Tremblay [4]

1 Science Systems and Applications Inc., Lanham, MD 20706, USA; zhipeng.wang@nasa.gov
2 NOAA/NESDIS/Center for Satellite Applications and Research, College Park, MD 20740, USA
3 Earth System Science Interdisciplinary Research Center (ESSIC), University of Maryland, College Park, MD 20740, USA; peter.beierle@noaa.gov
4 Global Science & Technology Inc., Greenbelt, MD 20770, USA; kun.zhang@noaa.gov (K.Z.); denis.tremblay@noaa.gov (D.T.)
* Correspondence: flavio.iturbide@noaa.gov

Abstract: Radiometric intercomparison between satellite remote sensing instruments has become an increasingly common practice to monitor the stability and even the accuracy of their radiance products. The assessment also enables the evaluation of calibration improvements made to these products, as well as the identification and resolution of remaining calibration inadequacies. In this paper, the radiance products of the Cross-track Infrared Sounder (CrIS), an interferometer-based hyperspectral IR sounder in low Earth orbit (LEO), is compared with the level-1b (L1b) radiance products of the infrared (IR) bands of the Advanced Baseline Imager (ABI), an imaging radiometer in geostationary (GEO) orbit. Two CrIS instruments are currently in operation on S-NPP and NOAA-20 satellites, respectively, and two ABI instruments are in operation on GOES-16 and GOES-17 satellites, respectively. Radiometric intercomparisons are performed between each CrIS-ABI pair. An established procedure by GSICS for such GEO-LEO instrument comparison is principally followed to emulate the radiance of ABI IR bands from CrIS spectra of the collocated pixels to be compared with the actual ABI radiance. Results show that the long-term time series of CrIS-ABI radiance bias have been stable within 0.2 K for nearly all ABI IR bands within a spectral range from 3.7 μm to 13.3 μm, except those with known calibration issues. Miscellaneous calibration events that had occurred to either instrument and altered the biases are identified and explained. While the main goal of the work is to support the on-orbit Cal/Val of CrIS, including the future JPSS-2/3/4 CrIS, such observations can also be referenced to further improve the calibration of ABI.

Keywords: infrared; intercomparison; validation; CrIS; remote sensing

Citation: Wang, Z.; Iturbide-Sanchez, F.; Beierle, P.; Zhang, K.; Tremblay, D. Validation of CrIS Radiometric Performance through Its Comparison to ABI. *Remote Sens.* **2022**, *14*, 876. https://doi.org/10.3390/rs14040876

Academic Editor: Michael Obland

Received: 2 January 2022
Accepted: 10 February 2022
Published: 12 February 2022

1. Introduction

The increasing availability of the space-borne remote sensing instruments for climate monitoring, weather forecasting, and various environmental applications populates the calibration strategy of radiometric intercomparison, a process to directly compare the measured radiances from collocated scenes from a pair of instruments and assess the radiance bias. Most of these instruments nowadays have their own capabilities of on-board calibration, making their intercomparison a powerful tool to cross-check the performance of, and improve the on-orbit calibration [1]. The instruments to be compared in this work are the Cross-Track Infrared Sounder (CrIS) on-board the Joint Polar Satellite System (JPSS) series satellites and the infrared (IR) bands of the Advanced Baseline Imager (ABI) on-board the Geostationary Operational Environmental Satellite - R series (GOES-R) satellites, both operated by the National Oceanic and Atmospheric Administration (NOAA). CrIS is a Fourier transform spectrometer based on a Michelson interferometer configuration. Currently, two CrIS instruments are in operation, one on the Suomi National Polar-orbiting Partnership (S-NPP) satellite launched in October 2011 and the other on the NOAA-20

satellite launched in November 2017. Both satellites fly on nearly sun-synchronous polar orbits at an ascending node equator crossing time of 13:30 p.m. locally, where the two spacecraft positions have a phase separation of 180 degrees within a common orbital plane. The 3rd CrIS is scheduled to launch on the JPSS-2 satellite no later than September 2022 and two more CrIS instruments are planned for JPSS-3 and JPSS-4. CrIS has three spectral bands: long-wave infrared (LWIR) band (650–1095 cm^{-1}), middle-wave infrared (MWIR) band (1210–1750 cm^{-1}), and short-wave infrared (SWIR) band (2155–2550 cm^{-1}). For each band, CrIS measures infrared (IR) spectra from the Earth Scene (ES) with a 3×3 detector array, corresponding to 9 field-of-views (FOVs) with a 14-km diameter footprint at nadir or one field-of-regard (FOR). With a scan mirror rotating in the cross-track direction, CrIS scans a 2200-kilometer swath width of $\pm$48 degrees. For each scan, CrIS collects 30 FORs of ES, two FORs of deep space (DS), that provides the detector background signal and two FORs of a reference blackbody called the Internal Calibration Target (ICT) [2].

The operational CrIS radiance products in format of Sensor Data Record (SDR) are produced by the JPSS Interface Data Processing Segment (IDPS) now in their full spectral resolution (FSR) of 0.625 cm^{-1} with a total 2211 spectral channels with Hamming apodization applied [3,4]. The CrIS SDR are assimilated into the global Numerical Weather Prediction (NWP) models, providing critical temperature and water vapor information for the improvement of weather forecasting and to enhance our understanding of the dynamics of the atmosphere [5,6]. The SDR products have also demonstrated the high measurement accuracy and long-term stability required to be used as top-of-atmosphere (TOA) IR radiance spectra references, supporting the calibration and validation (Cal/Val) of observations from other infrared sounders through radiometric intercomparison [7]. The calibration algorithms and coefficients of CrIS SDR have been upgraded throughout the mission to improve the data quality and to correct any on-orbit degradation of the instruments. Recently, the CrIS SDRs have been reprocessed at NOAA's National Environmental Satellite, Data, and Information Service (NESDIS) Center for Satellite Applications and Research (STAR), for both S-NPP and NOAA-20 missions with consistent and optimized calibration algorithm and coefficients using the off-line SDR processing code Algorithm Development Library (ADL) that mimics the operational IDPS. The ADL version for the reprocessing is 5.3.23, effectively equivalent to the software build of IDPS Block 2.1 Mx8. The reprocessed SDR are expected to show improved accuracy and stability in the radiometric, spectral and spatial domains [8,9]. Both the operational and reprocessed CrIS SDRs are assessed in this work through their intercomparison with ABI.

As the main payload on GOES-R, ABI remotely collects data in geosynchronous orbit of the land, ocean surface and atmosphere of the Earth's Western Hemisphere in higher radiometric sensitivity and spectral/spatial/temporal resolutions compared with the legacy GOES imager [10]. Two ABIs are in operation: one onboard the GOES-16 satellite launched in November 2016 that is currently located at 75.2° W longitude as GOES-East; the other one is onboard the GOES-17 satellite launched in March 2018 that is located at 137.2° W longitude as GOES-West. The two satellites can continuously generate a single full disk of Earth image every 10 or 15 min depending on their operational scan modes. Two more ABIs are scheduled to launch along with GOES-T, currently scheduled in March 2022 and GOES-U in 2024, respectively. ABI captures the Earth scene radiance in 16 spectral bands, covering a spectral range of 0.47–13.3 μm. Among them, bands 7–16 are categorized as IR bands. The ABI radiances are recorded in its level 1b (L1b) products. For IR bands, their L1b are also calibrated referencing an ICT nominally set at 302 K and its deep space (DS) view that provides the dark background for detectors. The specification of requirements (Spec.) for ABI IR radiometric accuracy is 1 K@300 K scene. Some key design parameters of the IR bands, including the center wavelength, nadir spatial resolution and typical applications, are summarized in Table 1 [11,12]. The calibration methodology of ABI is similar to other space-borne spectrometers, such as the Moderate Resolution Imaging Spectroradiometer (MODIS) instruments aboard NASA Terra and Aqua satellites [13] and the Visible Infrared Imaging Radiometer Suite (VIIRS) instruments aboard JPSS satellites [14,15].

Table 1. Key design parameters of ABI spectral bands.

Band	Wavelength (μm)	Resolution (km)	Typical Applications
1	0.47	1	Aerosols
2	0.64	0.5	Clouds
3	0.86	1	Vegetation
4	1.38	2	Cirrus
5	1.6	1	Snow/ice discrimination, cloud phase
6	2.2	2	Cloud particle size, snow, cloud phase
7	3.9	2	Fog, stratus, fire, winds
8	6.2	2	High-level water vapor, rainfall, winds
9	6.9	2	Mid-level water vapor, rainfall, winds
10	7.3	2	Low-level water vapor, winds
11	8.4	2	Cloud-top phase, dust, rainfall
12	9.6	2	Total column ozone, turbulence
13	10.3	2	Clouds, surface
14	11.2	2	Clouds, sea surface temperatures
15	12.3	2	Clouds, sea surface temperatures
16	13.3	2	Cloud-top pressure

Both as key instruments of NOAA's weather satellites, the quality of the radiance products of CrIS and ABI are critical to a wide range of downstream products and mission applications. The responsibility of our CrIS SDR algorithm Cal/Val science team of NOAA/NESDIS/STAR is to support the Cal/Val of the CrIS SDR product to maintain and improve its quality. As part of this effort, the capability of the CrIS-ABI intercomparison is developed to monitor the stability and assess the accuracy of the CrIS calibrated radiance. The main results are documented in this paper with the comparison extended to both the operational and reprocessed CrIS SDRs. This work is independent of the on-going efforts of other STAR Cal/Val teams originated with different perspectives or to support the Cal/Val of other instruments [16–19]. This paper is organized in the following way: after a brief overview of CrIS and ABI instruments, the methodology of the intercomparison and the criteria of the scene filtering are introduced in detail in Section 2. The results and the interpretation of the observed biases are provided for each CrIS-ABI pairs in Section 3. The applications of the radiometric intercomparison in identifying and assessing various CrIS and ABI calibration anomalies are presented in Section 4, followed by a summary in Section 5.

2. Methodology

The baseline LEO-GEO IR intercomparison methodology has been well established. In particular, the Global Space-based Inter-Calibration System (GSICS) standard approach is principally followed in this study [20], with our work limited on optimizing the criteria used for scene selection and the tuning of their thresholds through extensive sensitivity testing of the intercomparison results. The fundamental aspect of the intercomparison is that the thermal emission in the radiance spectrum from the same target is independent of measuring instruments. Therefore, if two instruments view the collocated targets at

the same viewing angles at the same time, and their detector responsivities are spectrally matched, the measured radiance, or the brightness temperature (BT) after the conversion by Planck's law, by the two instruments should be identical. Any detected bias can then be tied to the insufficiency of the calibration of either or both instruments. In reality, it is impossible for any two instruments, even those in the same family, to meet all these conditions, so the major challenges of the intercomparison are to optimize a series of criteria to choose the collocated targets and to properly transform the radiance products of one or both instruments to spatially and spectrally match them for direct comparison. Therefore, the actual implementation of the intercomparison depends on the instrument pair. The GSICS procedure followed to conduct the ABI-CrIS intercomparison is summarized in Table 2. To efficiently create the lifetime cross-comparison between two CrIS and two ABIs, it is critical to optimize each individual step to reduce the input data volume and computational complexity.

The input radiance files can be downloaded from NOAA STAR Central Data Repository (SCDR) or Comprehensive Large Array-data Stewardship System (CLASS) [21]. The data volume rates of CrIS SDR and ABI L1b (IR bands only) are approximately 43 GB and 29 GB per day, respectively. The satellite motions between CrIS and ABI around the time of their nadir overpass are shown in Figure 1 for an arbitrarily selected short period. GOES-R satellites are in GEO orbits, so the nadir positions of ABI are nearly static. S–NPP/NOAA-20 are in nearly Sun synchronous orbit and cross the Equator at 0130 and 1330 local time. This corresponds to 0630 UTC and 1830 UTC for GOES-16 nadir and 1030 UTC and 2230 UTC for GOES-17 nadir. For GEO-LEO instrument intercomparison, the collocated scenes are not limited to the nadir positions because the GEO instrument observe the Earth at a high altitude of 36,000 km at a fairly small viewing angle of between $-7.5°$ to $7.5°$. As a result, the collocated scenes could be found at a large spatial and temporal extents within a day.

The spatial element of CrIS radiance product is a detector's field-of-view (FOV) and the spatial element of ABI radiance product is a pixel. The geolocation information of CrIS FOVs is saved as latitude and longitude directly. The geolocation information of ABI pixels of IR bands is instead saved in the so-called fixed grid (FG) coordinates at 2 km nadir resolution and needs to be converted into latitude and longitude. With this information, the collocated CrIS and ABI scenes can be identified. The viewing angles of these collocated pixels/FOVs shall also be matched to minimize the differences in atmospheric optical depths along the line-of-sight (LOS) of the detectors. Again, the viewing angles for CrIS FOVs are directly accessible in the SDR and the viewing angles for ABI pixels need to be converted from the FG coordinates [22]. Currently, the viewing angle matching is only limited to the zenith angle which determines the atmospheric optical depths. The impact of azimuth angle mismatch is considered insignificant while adding the matching criteria greatly reduces the availability of the collocated scenes for comparison and thus increase the uncertainty of the results.

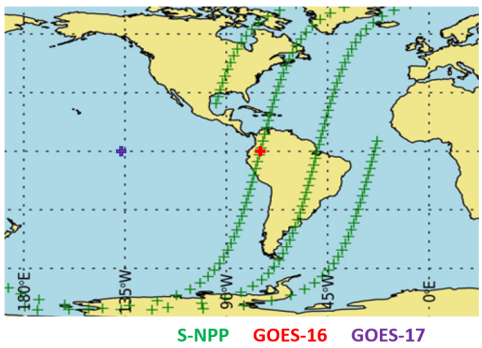

Figure 1. The nadir tracks of S-NPP satellites when it moves across the equator close the GOES-16 nadir (red cross).

Table 2. Procedure for the CrIS-ABI radiometric intercomparison.

Step	Description	Input	Output
1	Download selected CrIS/ABI radiance files	NOAA SCDR/CLASS	subset of radiance files containing collocated scenes
2	Collocate ABI pixels and CrIS FOVs for comparison	CrIS/ABI geolocation	CrIS spectrum (S_{CrIS}) and ABI radiance (L_{ABI}) at the collocated scenes
3	Pre-process S_{CrIS}	coefficients of gap-filling, Hamming apodization	gap-filled, apodized S_{CrIS}
4	Emulate L_{ABI} from S_{CrIS}	ABI SRF	emulated ABI radiance ($L'_{ABIfromCrIS}$)
5	Spatially aggregate L_{ABI} at CrIS FOV	L_{ABI}	aggregated ABI radiance at CrIS FOV (L''_{ABI})
6	Differentiate L''_{ABI} and $L'_{ABIfromCrIS}$	-	CrIS/ABI radiance bias
7	Filter out "bad" scenes	global surface-type map	final products of intercomparison

The radiances from both the CrIS and ABI collocated pixels need to be spatially and spectrally matched, to be differentiated directly. In the spatial domain, each CrIS FOV is 14 km in diameter at nadir, much larger than an ABI pixel, as is illustrated in Figure 2. Typically, there are 38–40 ABI pixels within a CrIS FOV for nadir scene. Therefore, the ABI radiance L_{ABI} is spatially aggregated into a CrIS FOV as L''_{ABI}. The spatial response function of the CrIS at sub-FOV level is not characterized so the aggregation is achieved by simply averaging the radiance of ABI pixels within a disk of 14 km in diameter. In the spectral domain, the CrIS spectrum at much higher resolution is multiplied with the spectral response function (SRF) of an ABI band before being integrated and normalized to calculate the emulated ABI radiance L'_{ABI}

$$L'_{ABIfromCrIS} = \frac{\sum_{\lambda_A}^{\lambda_B}(S_{CrIS} \times SRF_{ABI})}{\sum_{\lambda_A}^{\lambda_B} SRF_{ABI}}, \quad (1)$$

where λ_A and λ_B are the ABI band limits. This GSICS-standard of simulation of GEO band radiance as the convolution of LEO radiance spectra and GEO SRF [20] is calculated in CrIS sensor grid at 0.625 cm^{-1} resolution. The basic element of the CrIS-ABI radiance difference is then

$$\Delta L = L''_{ABI} - L'_{ABIfromCrIS}, \quad (2)$$

or in BT as

$$\Delta BT = BT''_{ABI} - BT'_{ABIfromCrIS}, \quad (3)$$

and the difference is per CrIS FOV per ABI band. The ABI SRFs are over-plotted with a sample CrIS spectrum illustrating the spectral ranges of the three CrIS spectral bands in Figure 3. As can be seen, the responses of ABI IR bands 7, 11 and 8 (barely) overlap with the CrIS spectral gaps, thus deteriorating the integration in Equation (1). The spectral gaps are filled a priori, using an algorithm and corresponding parameters developed in STAR [23]. It should be noted that the gap-filling parameters are derived from and for Hamming apodized CrIS spectra so Hamming apodization shall be applied to the unapodized CrIS spectrum S_{CrIS} read-out from SDR before being input to Equation (1)

$$S_{Apodized,i} = 0.23S_{i-1} + 0.54S_i + 0.23S_{i+1}, \quad (4)$$

where i is the CrIS channel number and S represents the unapodized spectra.

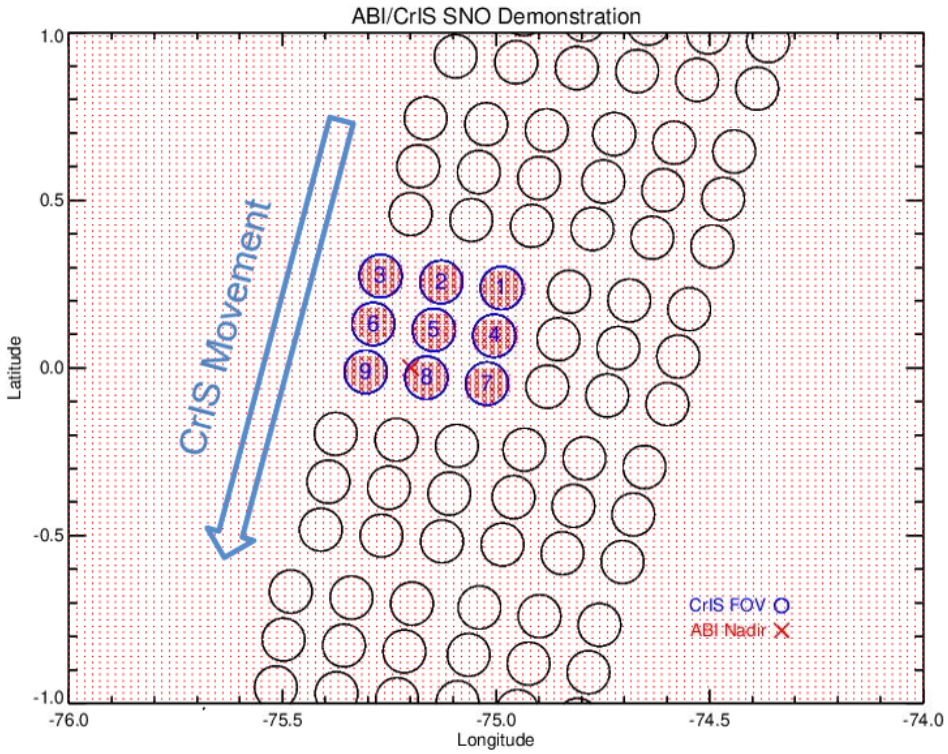

Figure 2. A schematic of the relative size and position between CrIS FOVs (black circles) and ABI pixels (red dots) at an SNO. The numbers in the CrIS FOVs are the indices of the FOVs.

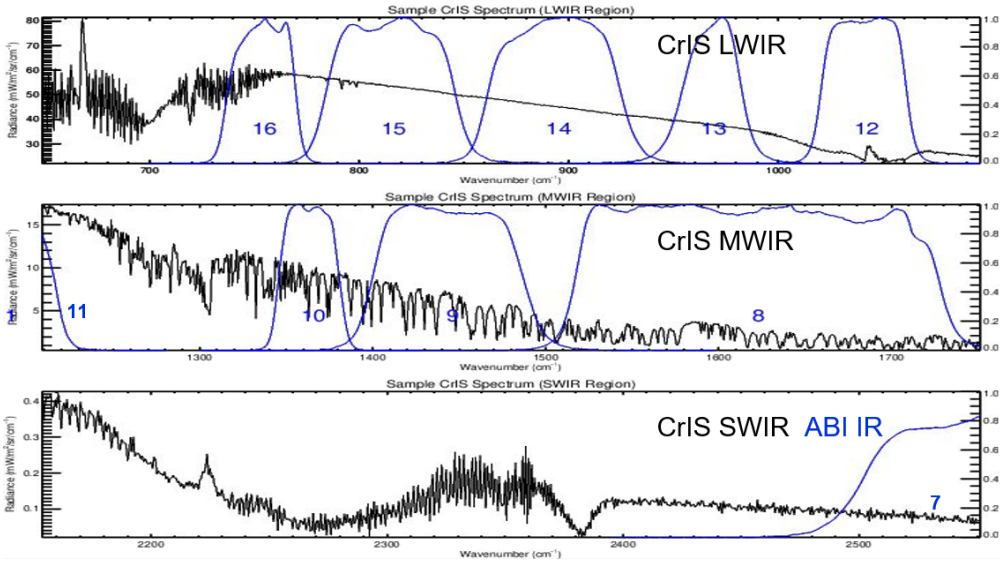

Figure 3. A sample CrIS spectrum at its FSR and the spectral response functions of ABI IR bands. The ABI band numbers are denoted in blue color.

The CrIS-ABI differences in Equations (2) and (3) can be calculated for all collocated pixels. Including larger amount of samples of collocated pixels could statistically reduce random error. However, including collocated pixels that include non-homogeneous scenes or large viewing angles, for example, could also yield to larger systematic errors, degrading the quality of the radiometric comparison. In this work, the scene filtering is based on

the following criteria: instrument scan angle for which smaller angle is preferred; scene homogeneity for which uniform scene is preferred, scene type for which ocean scene is preferred, difference between CrIS-ABI observation time for which shorter interval is preferred, difference between CrIS-ABI viewing angles for which small viewing angle difference is preferred. At last, the number of pixels after filtering should be large enough so that the random error in the daily average is reasonably small.

The typical thresholds of these criteria are summarized in Table 3. Among them, the scene homogeneity check is critical for this comparison: the standard deviation of the BTs of all the ABI pixels within a CrIS FOV is compared with the threshold of 0.5 K, an empirically determined value from the observation of the data. This is because the ABI pixels are at much higher spatial resolution than CrIS. The filtered scenes by the criteria, which can be referred to as "good" FOVs, are only a small subset of all the collocated FOVs. The collocated pixels identified by the criteria are plotted in Figure 4 for two orbits, one at descending node and one at ascending node, in a randomly selected day of 12 June 2021. The "good" FOVs are highlighted in green color. The number of good pixels varies from date to date, ranging from zero to more than a thousand. Various final products of CrIS-ABI intercomparison can be derived from these "good" FOVs. The thresholds in Table 3 can slightly differ among bands and instruments. For example, to increase the number of dates with more than 200 valid pixels to create a sustainable long-term trending, certain land pixels can be added to the "good" FOVs dataset for several short-wavelength bands with more stringent requirement in the observation time difference (240 s is reduced to 120 s). Also, to minimize the impact of the observation time difference, the ABI radiance before and after the CrIS measurement is temporally interpolated before being compared with the CrIS radiance if the time difference is greater than 60 s and the ABI temperature change is greater than 1 K.

Table 3. Thresholds of data filter criteria for ABI-CrIS intercomparison.

Criteria	Thresholds
Range of CrIS scan angle (in CrIS FOR number)	12–19
Scene homogeneity σT (K)	0.5
Observation time Diff. (s)	240
Scene type	Ocean
Local zenith angle (LZA) Diff. $\cos(\theta 1) - \cos(\theta 2)$	0.001
Minimum number of pixels per day	200

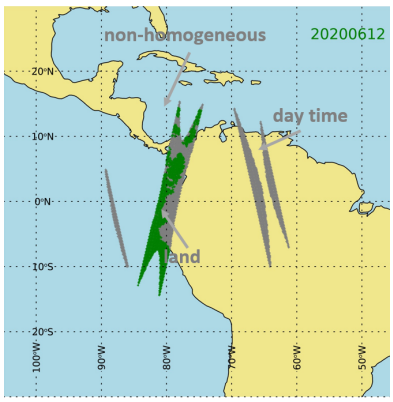

Figure 4. The positions of ABI-CrIS collocated pixels pre-selected for an arbitrary date. The pixels in grey color are further filtered out to be excluded from comparison by various criteria. The collocated pixels pre-selected for the day are highlighted in green color.

3. Results

3.1. CrIS vs. GOES-16 ABI

One of the main intercomparison products is the long-term time series of the daily-averaged BT differences between CrIS and ABI IR bands. The time series for S-NPP CrIS and GOES-16 ABI, between which the overlaps of mission lifetimes are the longest among all the CrIS-ABI pairs, are shown in Figure 5 for a period from 17 December 2017, right after GOES-16 moved to its current position, to 20 May 2021, right before the recent permanent failure of the S-NPP CrIS Electronics Side 2. Each data point is the average of BT differences of those filtered "good" collocated FOVs. Those days with less than 200 "good pixels" are excluded from the trending due to a potential larger random error. The daytime and nighttime observations are trended separately as a routine for the intercomparison of IR bands. The reflected sunlight during daytime can contaminate the thermal signal from the scene, in particular for shorter wavelength bands. In this case, the contamination is serious for ABI band 7 at 3.9 μm and negligible for other MWIR and LWIR bands. The scale of the y-axis in band 7 results is thus adjusted to better present how much the data fluctuation of the daytime band 7 result is. The results for all other bands have remained stable within a peak-to-peak range of $\pm$0.1 K and there is no noticeable gradual drift over time in the past three years. The radiometric biases for all bands are less than 0.2 K after June 2018, as summarized in Table 4. For several ABI bands, seasonal variations at small magnitude are observed from the trending, indicating the existence of radiometric bias associated with seasonal parameters.

The standard deviations of the BT difference are trended daily, as is shown in Figure 6. Their magnitudes are within a range of 0.1–0.25 K that is band-dependent. The random error of each point is then no more than $0.25/\sqrt{200}$, or 0.02 K. Therefore, the data variations exhibited in Figure 5 are mostly systematic error due to the methodology of the intercomparison. In particular, any mismatching between the CrIS and ABI observations of the collocated scenes in time, viewing angle, detector′ spectral and spatial responses leads to bias. In general, the uncertainty is larger for window bands and longer wavelength bands such as bands 11 and 13–16, which may suggest the anisotropic reflectance of the Earth surface is a contributing factor. Further investigation is underway. Because neither instrument is on-orbit traceable to absolute (SI) scale, the systematic error cannot be quantified from the intercomparison results alone. Overall, both the radiometric bias and the instability have remained much less than the Spec. of calibration accuracy of 1 K for the two instruments, suggesting the calibrations of CrIS and ABI, as well as their agreement, are in good condition for the trended periods.

The impacts of several noticeable events of either instrument can be observed. The calculation of the ICT temperature of GOES-16 ABI had been erroneous before June 2018 due to the incorrect coefficients used to convert the detector-counts to temperature conversion of the Platinum Resistance Thermometers (PRTs) that are embedded in the ICT [24]. The ICT temperature was lower estimated by nearly 0.2 K. Because the ICT temperature is the reference of the IR calibration, the error causes a calibration bias to all scenes. The magnitudes of the bias is scene-temperature dependent and is in a range of 0.1–0.2 K. The biases trending in Figure 5 clearly shows the correction of the coefficients operationally implemented in June 2018 reduced the CrIS-ABI bias for all bands.

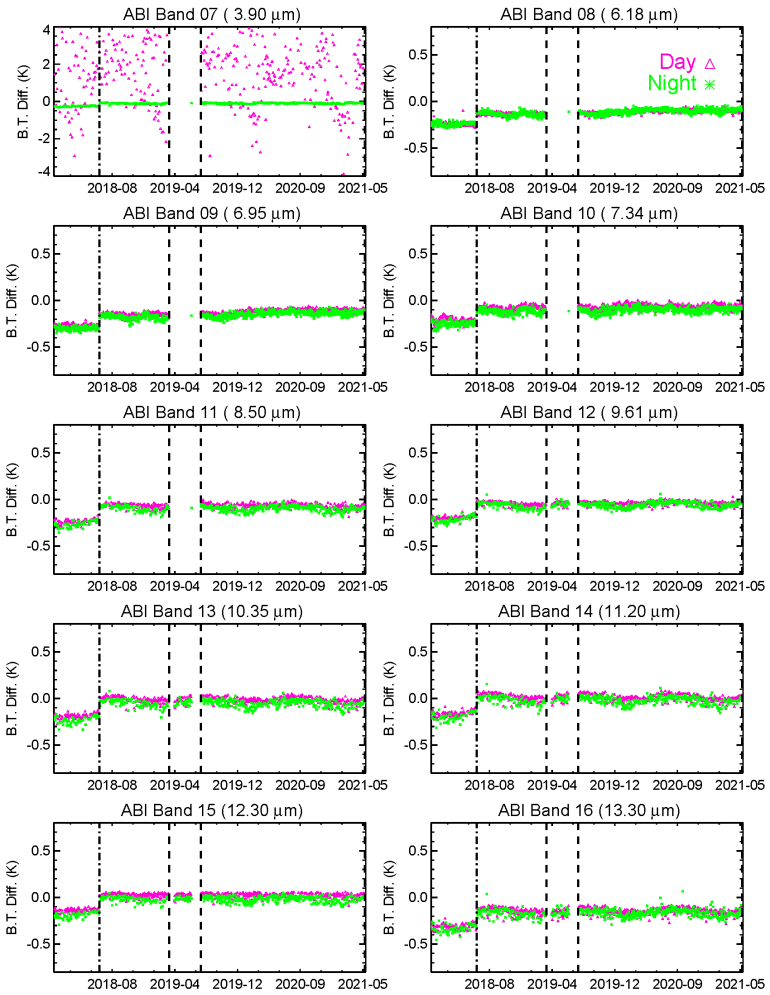

Figure 5. The long-term time series of the BT differences between S-NPP CrIS and GOES-16 ABI. The three vertical dashed lines denote major calibration events: Correction of ABI ICT temperature calculation in June 2018, the failure of CrIS MWIR band in March 2019, and the CrIS electronics Side-1/Side-2 switch in June 2019.

Table 4. A summary of GOES-16 ABI and S-NPP radiometric bias, derived from May 2020 to May 2021 night-time results.

ABI Band	ABI-CrIS Bias (Mean, K)	ABI-CrIS Bias (Stddev, K)
7	−0.10	0.08
8	−0.10	0.09
9	−0.13	0.08
10	−0.10	0.08
11	-0.10	0.09
12	−0.05	0.10
13	−0.06	0.10
14	−0.02	0.11
15	−0.02	0.10
16	-0.16	0.12

The vertical dashed lines in Figure 5 designate the time when the failure and recovery of the S-NPP CrIS MWIR band occurred. On 26 March 2019, the operational S-NPP CrIS SDR production stopped due to a failure of its MWIR band in Side-1 electronics. Later, the SDR production resumed without the MWIR data. Following a comprehensive risk assessment, the switch from primary to redundant Side-2 electronics was made on 24 June 2019 successfully recovering the full capabilities of the sensor [25]. As a result, data gaps between the two dates exist for ABI bands 8–11 corresponding to CrIS SWIR band.

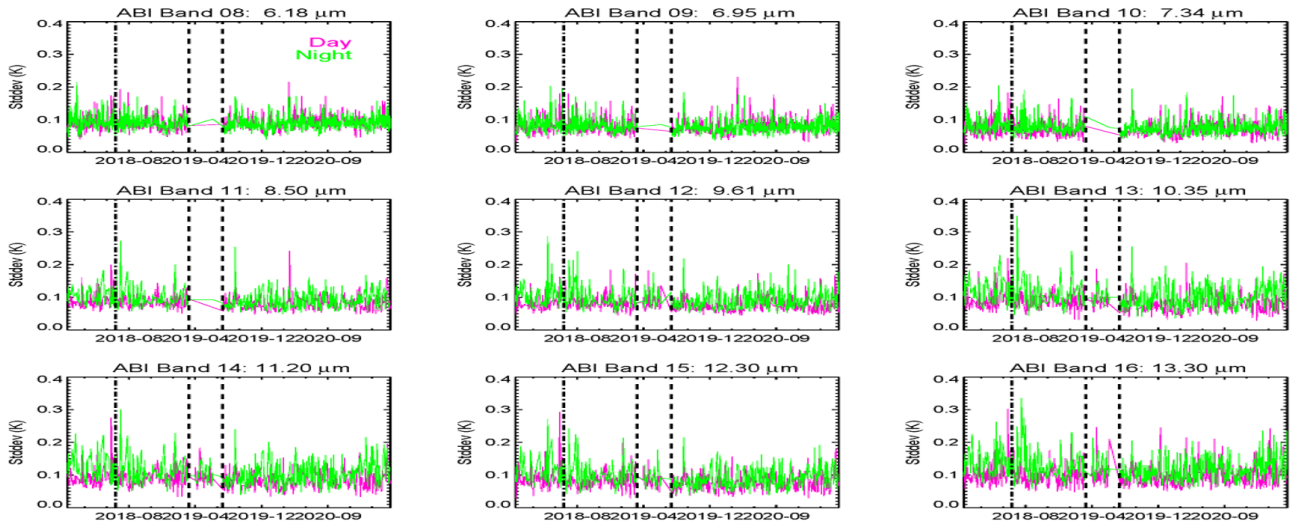

Figure 6. The long-term time series of the standard deviation of the BT differences between S-NPP CrIS and GOES-16 ABI.

The comparison of L''_{ABI} and $L'_{ABIfromCrIS}$ can also be presented at FOV level to study the dependency of the BT bias on scene temperatures. Excluding noise, a cold bias is detected as is shown in Figure 7. for nearly all bands. To extend the dynamic range of the observation, both land and ocean scenes are included to generate the figure. Similar bias has been observed between ABI and other IR sounding instruments such as the Infrared Atmospheric Sounding Interferometer (IASI), hinting the bias is more likely caused by the imperfect calibration of ABI. The comparison using radiance units shows the same bias pattern, which means the bias is caused by real calibration inadequacy, not the radiance to BT conversion by Planck's law. The root cause of the bias is unknown and subject to further investigation. It could be related to the resampling mechanism of the instrument, which means the radiance of an ABI pixel is not from direct measurement but a weighted interpolation of radiance from neighboring samples [22]. The interpolation potentially smoothes out the scene non-uniformity and twists the BT at the extreme temperatures at colder and warmer ends. The magnitude of the bias is approximately 1 K@200 K scene from the results. For direct comparison, the ABI Spec. of radiometric accuracy of 1 K shall be scaled from 300 K scene to 200 K scene by multiplying by the ratio of the derivative of Planck's law $\delta L/\delta T_{200K}$ and $\delta L/\delta T_{300K}$. The results are wavelength-dependent and range from approximately 2 K for band 16 and 10 K for band 7. This means the bias observed in the intercomparison results is much smaller than the specification or its equivalent. For ABI window bands 11, 13–15 and potentially for other bands, warm biases are observed at the higher end of the temperature range that corresponds to land scenes. The exact reason of the bias is to be investigated.

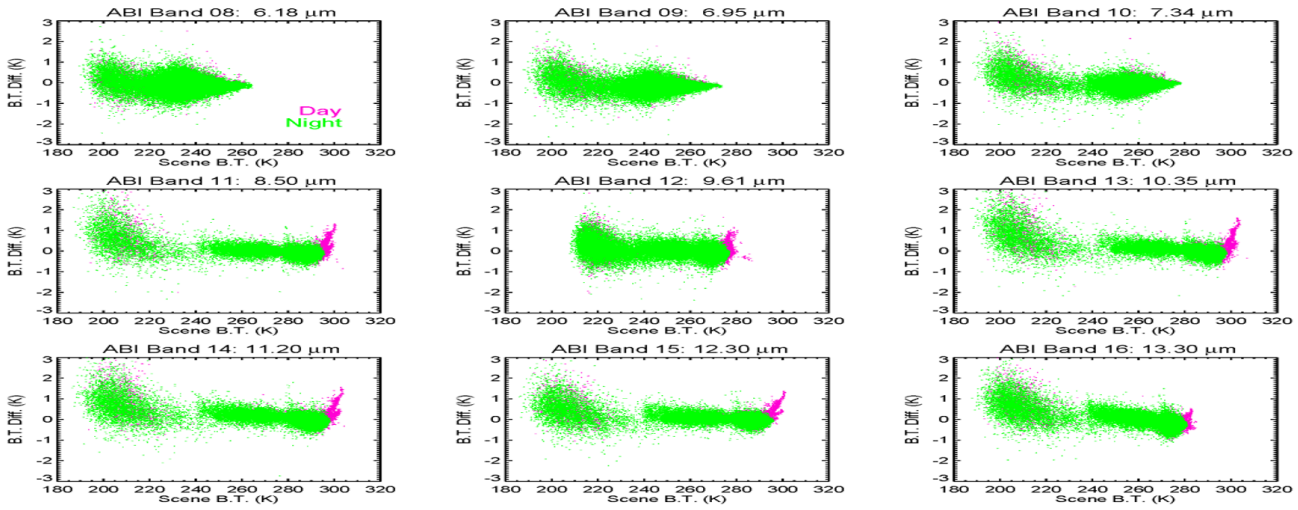

Figure 7. The FOV-level BT difference between S-NPP CrIS and GOES-16 ABI. Band 7 is excluded from trending for its large uncertainty.

3.2. CrIS vs. GOES-17 ABI

The long-term time series of daily-averaged BT differences between S-NPP CrIS and GOES-17 ABI are generated for ABI bands and shown in Figure 8. The interpretation of the intercomparison results for GOES-17 ABI will be much more complicated since its IR bands operate at dynamic thermal environment and instrument settings due to its loop heat pipe (LHP) anomaly [26,27]. The discontinuities and gaps in the trending are almost exclusively the results of the inadequacy of ABI calibration. Almost every day, the IR detectors of ABI bands 8-16 alternatively operate at gain set I (higher gain) during daytime and gain set III (lower gain) during nighttime. In general, the quality of the L1b radiance product is better when operating at the gain set I period than the gain set III period, in terms of accuracy, stability and noise level, so the trending is more stable for the daytime than nighttime, in contrast to the intercomparison results of most of other instrument pairs. The bias between the two instruments, mostly noticeable for band 16, is at least partly because the ABI SRFs operationally implemented are characterized at a focal plane module (FPM) temperature of 60 K and thus inconsistent with the actual SRFs after the operational FPM temperature was lifted to 81 K and higher. Also, the noise level of ABI band 16 is much larger than other IR bands so the radiance of those ABI pixels within a CrIS FOV are too noisy to pass the scene homogeneity test. Therefore, the nighttime results are almost nonexistent for the band. All these results indicate S-NPP CrIS is a good reference to identify and assess the calibration inadequacy of ABI. On the other side, the calibration of GOES-16 ABI is more stable than GOES-17 ABI, making it a better reference for CrIS assessment when needed.

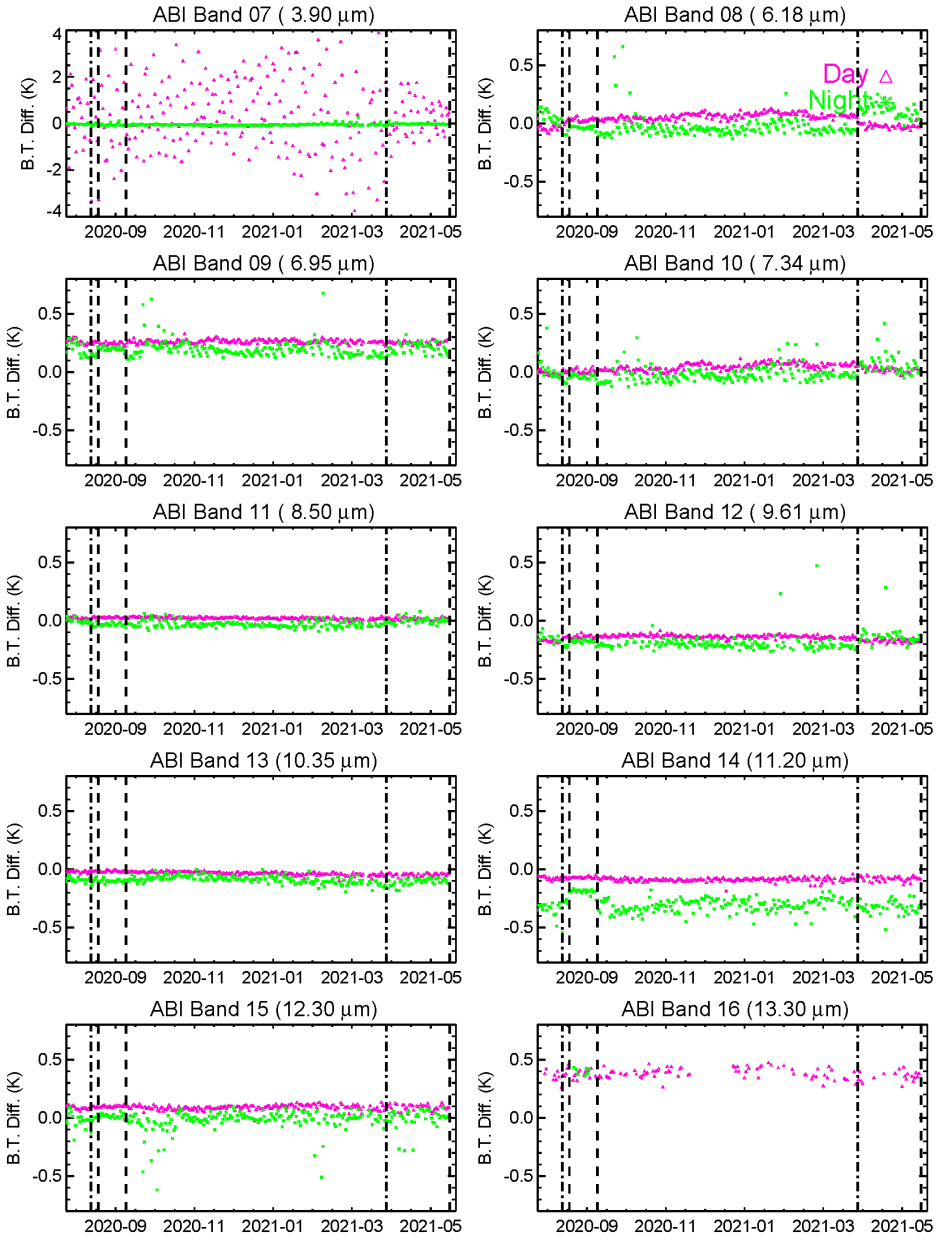

Figure 8. The long-term time series of the standard deviation of BT differences between S-NPP CrIS and GOES-17 ABI.

3.3. S-NPP CrIS vs. NOAA-20 CrIS through Double Difference

The intercomparison between NOAA-20 CrIS and the two ABIs is nearly indiscernible to S-NPP so the results are not separately presented. Using the stable GOES-16 ABI as a bridging sensor, the calibration differences between S-NPP and NOAA-20 CrIS can be characterized as

$$\Delta BT_{S-NPP/N-20} = \Delta BT_{G-16/N-20} - \Delta BT_{G-16/S-NPP}, \quad (5)$$

where ΔBT on the right side of the equation is defined in Equation (3). The trending of the double difference is presented in Figure 9. The bias between the two instrument is smaller than 0.1 K for all bands and there is no noticeable temporal drift, even though the trending is much noisier for longer-wavelength bands. The comparison again demonstrates the excellent quality of the calibrated SDR of both CrIS instruments.

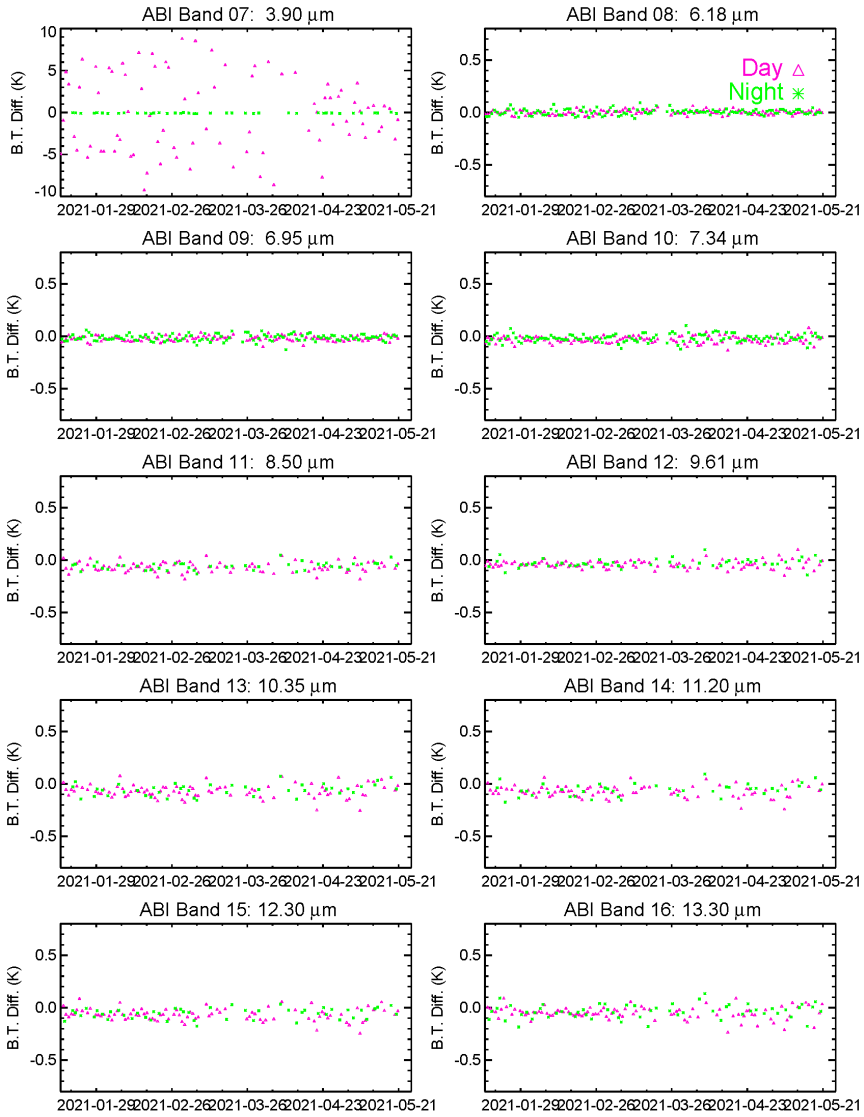

Figure 9. The BT differences between S-NPP CrIS and NOAA-20 CrIS (NOAA-20 minus S-NPP) using GOES-16 ABI as a common reference.

3.4. Uncertainty

The uncertainty of the CrIS-ABI intercomparison is propagated from the uncertainties of the CrIS radiance, the ABI radiance and the intercomparison methodology. The former two sources reflect the uncertainties of the calibration of the instruments and are thus truly important for their performance assessment. Without an SI-traceable absolute calibration standard, the result of CrIS-ABI BT bias itself cannot separate error sources from CrIS or ABI so the knowledge on the calibration of either or both instruments are necessary to interpret the results, as is done in the above and below discussions. These interpretations can be viewed as the identification of the related error sources. Ideally, the uncertainty of the methodology shall be as small as possible to be neglected. The impacts of the mismatching of pixel collocation, observation time, and viewing angles are scene dependent and it is assumed that the majority of these impacts are random errors that can be minimized by the inclusion of a large set of collocated pixels. Therefore, the statistics of the BT bias between GOES-16 ABI and S-NPP CrIS, two well-calibrated instruments, in Table 4 can be deemed as the upper-bound of the uncertainty of the CrIS-ABI intercomparison methodology. The larger bias observed between GOES-17 ABI and S-NPP CrIS can then be attributed to GOES-17 ABI alone if the uncertainty from the methodology is comparable for the two

intercomparisons. In-depth analysis of the uncertainty of intercomparison methodology is beyond the scope of this study.

4. Applications in Assessing CrIS Anomalies

The GOES-T, or GOES-18 if renamed upon reaching its orbit, ABI is currently scheduled to be launched in March 2022 and the JPSS-2 (NOAA-21) CrIS is scheduled to be launched in September 2022. The intercomparison software developed can be conveniently extended to these incoming ABI and CrIS to support their calibration. As a GEO instrument, ABI is scanning the whole Western Hemisphere every 10 minutes in its current mode 6 setting. This ensures enough collocated pixels between CrIS and ABI to conduct intercomparison on a daily basis. On the other hand, the collocated pixels between LEO instruments are either limited, such as IASI vs. CrIS or AIRS vs. CrIS, or non-existing such as S-NPP CrIS vs. NOAA-20 CrIS, their intercomparison cannot be updated as frequently. This makes CrIS-ABI intercomparison a powerful tool to timely identify issues with the instrument as well as its calibration and particularly benefits the initial on-orbit instrument Cal/Val. Examples are provided below to demonstrate how the intercomparison results can be applied to the assessment of the CrIS SDR quality.

4.1. SDR Quality during S-NPP LWIR Failure

The SNPP CrIS instrument, which had been operating at its electronics Side-2 since the failure of its Side-1 MWIR band, experienced a LWIR Signal Processor failure on 21 May 2021. That stopped the production of the SDR by IDPS. The measurements of its MWIR and SWIRs are still available so there is a need to assess their quality to decide whether the SDRs of MWIR and SWIR can still be produced. Using the off-line SDR processing ADL that includes the same CrIS SDR processing code as that of the operational code at IDPS, the test SDR are produced off-line and compared with GOES-16 ABI. The comparison results in Figure 10 clearly show stable trending before and after the failure for ABI bands 8-10 that corresponds to CrIS MWIR band. Together with other independent assessment results, IDPS resumes the operational production of SDRs on 27 May 2021 after switching back to its Side-1 electronics.

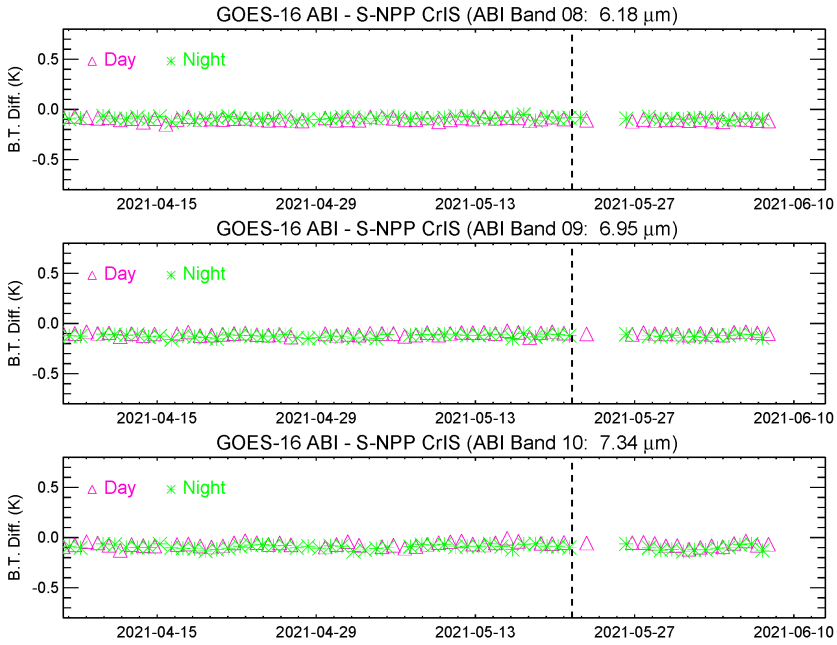

Figure 10. The intercomparision between GOES-16 ABI and S-NPP CrIS before and after the 21 May 2021 S-NPP CrIS LWIR failure in MWIR spectral range.

4.2. Impact of Lunar Intrusion

In the long-term BT difference trending between S-NPP CrIS and GOES-16 ABI, two significant data outliers are detected for ABI band 8 on 29 December 2017 and 25 April 2018, respectively, as is highlighted in Figure 11. Further investigation shows the CrIS radiances of some collocated FOVs used in the intercomparison are noticeably lower than other FOVs as well as the ABI radiances. The CrIS DS window sizes shrink during the period, suggesting an intrusion of the Moon into the DS that was not detected appropriately. As a result, the DS signal is contaminated by the Moon light and overestimated, leading to a negative bias of the calibrated radiance. Improved lunar intrusion detection algorithm and thresholds were implemented in IDPS operation on 17 December 2018 and 10 May 2019, respectively [8]. Such outliers have not occurred since. Also, the outliers are non-existent when using the reprocessed CrIS SDR as inputs for CrIS-ABI intercomparison, which are produced by off-line ADL with the latest calibration algorithms, including the lunar intrusion detection algorithm backwardly applied to the production of SDRs. Direct comparison between the operational SDR and reprocessed SDR in Figure 12 shows the operational SDRs are colder than reprocessed SDR for certain FOVs.

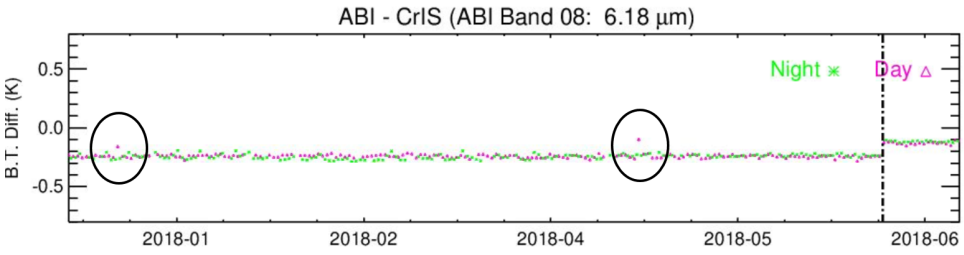

Figure 11. The BT differences between S-NPP CrIS and GOES-16 ABI for a six-month period before the lunar intrusion rejection algorithm was implemented in operation.

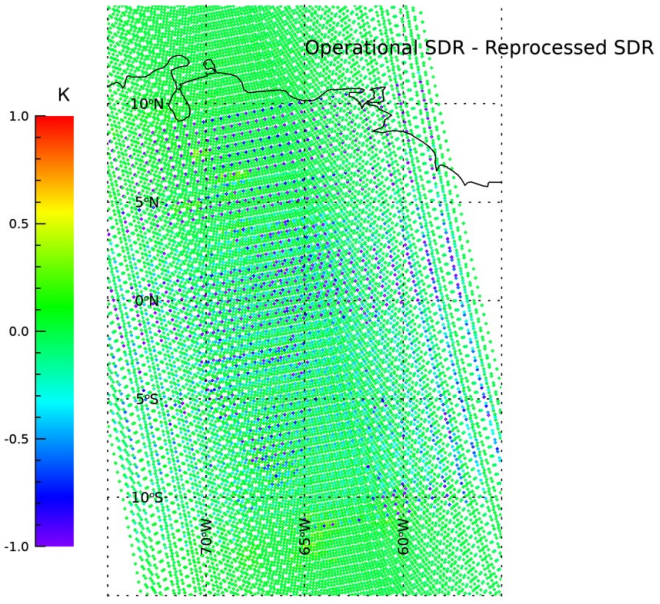

Figure 12. The BT differences between the operational and reprocessed S-NPP CrIS SDR during an lunar intrusion event on 25 April 2018. The color scale is from −1 K to 1 K while the actual BT differences exceed this range.

5. Conclusions

An ABI-CrIS intercomparison tool is independently developed to support the on-orbit Cal/Val of S-NPP and NOAA-20 CrIS instruments. Both CrIS instruments are radiometrically compared with GOES-16 and GOES-17 ABI with the their BT bias results presented

in terms of both their temporal trending and radiometric dependency. The stability and likely the accuracy of the CrIS SDR products are estimated to reach the initial estimation of 0.1 K level for daily-averaged values, that is well below the radiometric calibration Spec. The more stable GOES-16 ABI is also used as a radiometric transfer target to bridge the comparison between S-NPP and NOAA-20 CrIS through double difference. Combined with the knowledges about CrIS and ABI calibrations from our regular Cal/Val supporting efforts, the observed CrIS-ABI BT biases are concluded as mostly being tied to the calibration issues with ABI, not CrIS. It is demonstrated that the CrIS-ABI intercomparison can provide day-to-day monitoring of the CrIS instrument health, as well as its calibration stability and accuracy at 0.1 K level, and the results can be referenced to detect and diagnose numerous types of calibration anomalies. The intercomparison will be routinely performed for existing instruments and extended to future ones upon their launch.

Author Contributions: Conceptualization and methodology, Z.W. and F.I.-S.; software and formal analysis, Z.W.; validation, P.B., K.Z. and D.T.; writing—original draft preparation, Z.W. and F.I.-S.; writing—review and editing, P.B., K.Z. and D.T.; visualization, P.B.; supervision, project administration and funding acquisition, F.I.-S. All authors have read and agreed to the published version of the manuscript.

Funding: This study was partially funded by grant NA19NES4320002 (Cooperative Institute for Satellite Earth System Studies -CISESS) at the University of Maryland through the Joint Polar Satellite System (JPSS) Program.

Institutional Review Board Statement: Not applicable.

Informed Consent Statement: Not applicable.

Data Availability Statement: The CrIS and ABI L1b data used in the paper are publicly available at NOAA CLASS https://www.avl.class.noaa.gov/ (accessed on 4 January 2022).

Acknowledgments: The authors would like to thank the contributions of other members of NOAA STAR and JPSS program. The scientific results and conclusions, as well as any views or opinions expressed herein, are those of the author(s) and do not necessarily reflect those of NOAA or the Department of Commerce. This work was supported by the Joint Polar Satellite System Program Office.

Conflicts of Interest: The authors declare no conflict of interest.

References

1. Heidinger, A.K.; Cao, C.; Sullivan, J.T. Using Moderate Resolution Imaging Spectrometer (MODIS) to calibrate advanced very high resolution radiometer reflectance channels. *J. Geophys. Res. Atmos.* **2002**, *107*. doi: 10.5194/amt-13-4619-2020. [CrossRef]
2. Han, Y.; Revercomb, H.; Cromp, M.; Gu, D.; Johnson, D.; Mooney, D.; Scott, D.; Strow, L.; Bingham, G.; Borg, L.; et al. Suomi NPP CrIS measurements, sensor data record algorithm, calibration and validation activities, and record data quality. *J. Geophys. Res. Atmos.* **2013**, *118*, 12734–12748. [CrossRef]
3. Han, Y.; Chen, Y. Calibration algorithm for cross-track infrared sounder full spectral resolution measurements. *IEEE Trans. Geosci. Remote Sens.* **2018**, *56*, 1008–1016. [CrossRef]
4. Strow, L.L.; Motteler, H.; Tobin, D.; Revercomb, H.; Hannon, S.; Buijs, H.; Predina, J.; Suwinski, L.; Glumb, R. Spectral calibration and validation of the Cross-track Infrared Sounder on the Suomi-NPP satellite. *J. Geophys. Res. Atmos.* **2013**, *118*, 12486–12496. [CrossRef]
5. Eresmaa, R.; Letertre-Danczak, J.; Lupu, C.; Bormann, N.; McNally, A.P. The assimilation of Cross-track Infrared Sounder radiances at ECMWF. *Q. J. R. Meteorol. Soc.* **2017**, *143*, 3177–3188. [CrossRef]
6. Dahoui, M.; Isaksen, L.; Radnot, G. Assessing the impact of observations using observation-minus-forecast residuals. *ECMWF Newsl.* **2017**, *152*, 27–31.
7. Goldberg, M.; Ohring, G.; Butler, J.; Cao, C.; Datla, R.; Doelling, D.; Gartner, V.; Hewison, T. The global space-based intercalibration system. *Bull. Am. Meteorol. Soc.* **2011**, *92*, 467–475. [CrossRef]
8. Chen, Y.; Tremblay, D.; Wang, L.; Iturbide-Sanchez, F. Improved Lunar Intrusion Detection Algorithm for the CrIS Sensor Data Record. *IEEE Trans. Geosci. Remote Sens.* **2019**, *58*, 1134–1145. [CrossRef]
9. Iturbide-Sanchez, F.; Wang, Z.; Zhang, K.; Tremblay, D.; Lynch, E.; Beierle, P.; Chen, Y. Toward high-quality and long-term stability S-NPP and NOAA-20 cross-track infrared sounder sensor data record products. In Proceedings of the 2021 IEEE International Geoscience & Remote Sensing Symposium, Online, 14 October 2021.
10. Schmit, T.J.; Gunshor, M.M.; Menzel, W.P.; Gurka, J.J.; Li, J.; Bachmeier, A.S. Introducing the Next-generation Advanced Baseline Imager on GOES-R. *Bull. Am. Meteorol. Soc.* **2005**, *86*, 1079–1096. [CrossRef]

11. Kalluri, S.; Alcala, C.; Carr, J.; Griffith, P.; Lebair, W.; Lindsey, D.; Race, R.; Wu, X.; Zierk, S. From Photons to Pixels: Processing Data from the Advanced Baseline Imager. *Remote Sens.* **2018**, *10*, 177. [CrossRef]
12. Schmit, T.J.; Lindstrom, S.S.; Gerth, J.J.; Gunshor, M.M. Applications of the 16 Spectral Bands on the Advanced Baseline Imager (ABI). *J. Oper. Meteorol.* **2018**, *6*, 33–46. [CrossRef]
13. Xiong, X.; Wu, A.; Wenny, B.N.; Madhavan, S.; Wang, Z.; Li, Y.; Chen, N.; Barnes, W.L.; Salomonson, V.V. Terra and Aqua MODIS Thermal Emissive Bands On-Orbit Calibration and Performance. *IEEE Trans. Geosci. Remote Sens.* **2015**, *53*, 5709–5721. [CrossRef]
14. Cao, C.; Xiong, J.; Blonski, S.; Liu, Q.; Uprety, S.; Shao, X.; Bai, Y.; Weng, F. Suomi NPP VIIRS sensor data record verification, validation, and long-term performance monitoring. *J. Geophys. Res. Atmos.* **2013**, *118*, 11664–11678. [CrossRef]
15. Xiong, X.; Butler, J.; Chiang, K.; Efremova, B.; Fulbright, J.; Lei, N.; McIntire, J.; Oudrari, H.; Sun, J.; Wang, Z.; et al. VIIRS on-orbit calibration methodology and performance. *J. Geophys. Res. Atmos.* **2013**, *119*, 5065–5078. [CrossRef]
16. Wang, Z.; Iturbide-Sanchez, F.; Chen, Y.; Lynch, E.; Beierle, P. Assessment of Radiometric Calibration Consistency between CrIS and ABI IR Bands through Intercomparison. In Proceedings of the 101th AMS Annual Meeting, Online, 14 January 2021.
17. Jin, X.; Yan, B.; Sun, N.; Iturbide-Sanchez, F. Improving SNPP and NOAA-20 CrIS LTM Intersensor Radiometric Bias Assessment by Using Interpolating ABI Measurements as Transfer. In Proceedings of the 101th AMS Annual Meeting, Online, 14 January 2021.
18. Wang, L.; Sun, N.; Yan, B. NOAA ICVS/GSICS Recent Updates for GEO-LEO IR Inter- Calibration. In Proceedings of the GSICS Annual Meeting, Online, 8 April 2021.
19. NOAA GOES-R CWG. Available online: https://www.star.nesdis.noaa.gov/GOESCal/index.php (accessed on 4 January 2022).
20. Hewison, T.J.; Wu, X.; Yu, F.; Tahara, Y.; Hu, X.; Kim, D.; Koenig, M. GSICS Inter-Calibration of Infrared Channels of Geostationary Imagers Using Metop/IASI. *IEEE Trans. Geosci. Remote Sens.* **2013**, *51*, 1160–1170. [CrossRef]
21. NOAA CLASS. Available online: https://www.class.noaa.gov/ (accessed on 4 January 2022).
22. GOES-R Series Product Definition and Users' Guide. 2018. Available online: https://www.goes-r.gov/resources/docs.html (accessed on 4 January 2022).
23. Xu, H.; Chen, Y.; Wang, L. Cross-Track Infrared Sounder Spectral Gap Filling Toward Improving Intercalibration Uncertainties. *IEEE Trans. Geosci. Remote Sens.* **2018**, *57*, 509–519. doi: 10.1109/TGRS.2018.2857833. [CrossRef]
24. Yu, F.; Wu, X.; Yoo, H.; Qian, H.; Shao, X.; Wang, Z.; Iacovazzi, R. Radiometric calibration accuracy and stability of GOES-16 ABI Infrared radiance. *J. Appl. Remote Sens.* **2021**, *15*, 048504. [CrossRef]
25. Iturbide-Sanchez, F.; Strow, L.; Tobin, D.; Strow, L.; Wang, L.; Mooney, D.L.; Johnson, D. Recalibration and Assessment of the SNPP CrIS Instrument: A Successful History of Restoration After Midwave Infrared Band Anomaly. *IEEE Trans. Geosci. Remote Sens.* **2022**, *60*, 1–21. doi: 10.1109/TGRS.2021.3112400. [CrossRef]
26. Naarden, J.V.; Lindsey, D. Saving GOES-17, 2019. Available online: https://aerospaceamerica.aiaa.org/departments/saving-goes-17 (accessed on 4 January 2022).
27. Wang, Z.; Wu, X.; Yu, F.; Fulbright, J.P.; Kline, E.; Yoo, H.; Schmit, T.J.; Gunshor, M.M.; Coakley, M.; Black, M.; et al. On-orbit calibration and characterization of GOES-17 ABI IR bands under dynamic thermal condition. *J. Appl. Remote Sens.* **2020**, *14*, 034527. doi: 10.1117/1.JRS.14.034527. [CrossRef]